$E0$ decay from the first excited 0^+ state in ^{162}Yb

N. Blasi,[1] L. Guerro,[2,3] A. Saltarelli,[2,3] O. Wieland,[1] and L. Fortunato[4,5]

[1]*INFN, Sezione di Milano, via Celoria 16, 20133 Milano, Italy*

[2]*Division of Physics, School of Science and Technology, Università di Camerino, via Madonna delle Carceri, 62032 Camerino (MC), Italy*

[3]*INFN-Sezione di Perugia, via A. Pascoli, 06123 Perugia, Italy*

[4]*Dipartimento di Fisica e Astronomia "Galileo Galilei," Università di Padova, via Marzolo, 8, 35131 Padova, Italy*

[5]*INFN, Sezione di Padova, via Marzolo, 8, 35131 Padova, Italy*

(Received 15 May 2013; published 19 July 2013)

Excited states in ^{162}Yb were populated via β^+/EC decay and were studied via conversion electrons and γ-ray spectroscopy at the Tandem Accelerator in the INFN Laboratory Nazionali del Sud in Catania, Italy. Conversion electrons were detected by a miniorange spectrometer with a transmission energy window that ranged from 500 to 1300 keV. The $E0$ decay of the first excited state at 1006 keV to the ground state was observed, and a $X(E0/E2)$ value was deduced. The value is compared to a few IBM-1 calculations by using the ECQF formalism or the full Hamiltonian in multipole expansion. Calculations turn out to be quite sensitive to properties related to nuclear shape.

DOI: 10.1103/PhysRevC.88.014318 PACS number(s): 23.20.Nx, 27.70.+q, 21.60.Fw

I. INTRODUCTION

Collective nuclei in the mass region of $Z = 50$–82 have always been of great interest because of the evidence of structure evolutions from weakly to well-deformed or γ-soft shapes as a function of N, Z, and A. The introduction of the interacting boson approximation (IBA) in the late years of the 1970s has since triggered a large number of calculations in this mass region due to the flexibility of the model to describe not only exact symmetries that correspond to different geometrical models, but also transitional cases within the same framework. Further developments of the model, which include the extension to a proton-neutron formulation, the inclusion of higher degrees of freedom, such as g bosons or s' bosons, the study of the underlying microscopic structure, the use of a simplified Hamiltonian to reduce the number of parameters, etc., were applied in this mass region. The most recent development of the model is inspired by the exact parameter-free solution of the Bohr collective Hamiltonian at the critical point of shape phase transitions between spherical and γ-soft shapes E(5) [1] or between spherical and axially deformed shapes X(5) [2]. Typical signatures for an X(5) nucleus are the following: (i) The ratio of the energies of the 4_1^+ and the 2_1^+ states E_{4+}/E_{2+} is equal to 2.91; (ii) the energy ratio of the 0_2^+ and 2_1^+ states E_{0+}/E_{2+} is equal to 5.67; (iii) the ground state $B(E2; I \to I-2)$ values increase at a rate intermediate between vibrator and rotor. ^{152}Sm [3], ^{154}Gd [4], and ^{156}Dy [5] were indicated as possible candidates. The X(5) solution is obtained by choosing a square-well potential in the Bohr Hamiltonian and an infinite number of particles, which might be considered unrealistic, but critical point and shape coexistence can also be studied within algebraic approaches, such as the IBA, that incorporate a finite boson number. McCutchan *et al.* [6] investigated the connection between X(5) and IBA and found that energy spectra that satisfy the X(5) scheme do not correspond to the shape coexistence region for boson numbers smaller than 25. On the other hand, the critical point is expected to hardly be found in nature since the shape variation is a function of a discrete quantity, i.e., the nucleon number. Nevertheless, a nucleus can be close enough to the critical point to exhibit the main signatures predicted by the model, and a large number of studies have searched for critical point nuclei in this mass region. Also, ^{162}Yb has been proposed as a X(5) candidate after the recent revision of the level scheme [7] with the elimination of a previously reported 0^+ state at 606 keV. A partial level scheme of ^{162}Yb is shown in Fig. 1. It should be noted, however, that ground state $B(E2)$ values are not reproduced by X(5), which are very close to the rotational limit values, which leaves open the question whether this nucleus lies in the shape coexistence region.

In addition to the energy of the 0_2^+ state, the monopole strength $\rho^2(E0)$ to the ground state would be a useful test for the critical point [8] since it is related to the nuclear shape. An overview over shape coexistence and excited 0^+ states can be found in Ref. [9] where strong $\rho^2(E0)$ are indicated as fingerprints for the presence of shape coexistence. Unfortunately, the measure of $\rho^2(E0)$ requires the lifetime measurement of the 0_2^+ state, which is often very hard to populate with sufficient intensity. The commonly used quantity $X(E0/E2)$, i.e., the ratio between $E0$ and $E2$ transition intensities, which deexcites the 0_2^+ state, has the disadvantage to theoretically imply two distinct parameters in the $E2$ and in the $E0$ operators. The $E2$ effective charge e_2 can be fixed with a fit on the ground-state band $B(E2)$ values, but there are only very few known $E0$ transitions [10], if not only one, such as in ^{162}Yb, or none. Furthermore, the $X(E0/E2)$ value is a ratio between two quantities usually rather small where one is the inhibited $E0$ transition and the other is the $E2$ transition from the β to the ground-state band.

Recently, Zerguine *et al.* [11] suggested that the mean-square charge radius, isotope and isomer shifts, and the monopole operator may be treated in a consistent way so that the same parameters can be used. They performed calculations over all isotopes in the $A \approx 150$–170 region from samarium to tungsten by using a multipole expansion of the IBA-1 Hamiltonian and by allowing only the quadrupole parameter to vary along each isotope chain. However, the lighter

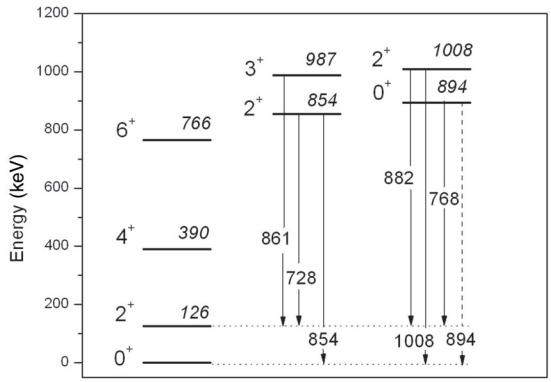

FIG. 1. Partial level scheme of ^{162}Yb that shows transitions observed in the present experiment. The $E0$ transition is indicated by a dashed arrow. Energies are in keV.

Yb isotopes were not well reproduced. Other authors, Chou *et al*. [12] and McCutchan *et al*. [13], performed extensive calculations in this region by using different approaches, which obtained a better agreement for the Yb isotopes. In particular, McCutchan *et al*. [13] also mapped the trajectory of each isotope chain in the symmetry triangle and found that in the Yb isotope chain, contrary to Gd, Dy, and Er isotopes, the γ softness decreases with neutron number.

In order to get more insight on the structure of the nucleus ^{162}Yb, we measured, for the first time, the $E0$ transition from the 0_2^+ state at 1006 keV to the ground state. Conversion electrons were recorded together with γ rays, and the $X(E0/E2)$ value could be deduced. The experimental setup and results are described in Sec. II. In Sec. III, the IBA-1 calculations mentioned above were extended to describe isotope shifts for the nuclei forms ^{160}Yb to ^{168}Yb, and $X(E0/E2)$ values then were calculated by using the same parameters and were compared to the experimental value. It turns out that isotope shifts and $X(E0/E2)$ values are strongly related and are quite sensitive to nuclear shape variations but also are sensitive to the choice of the Hamiltonian parameters. A new calculation that uses the full IBA-1 Hamiltonian is presented.

II. EXPERIMENT

A. The experimental setup

The experiment was performed at the INFN *Laboratori Nazionali del Sud* (LNS) in Catania. Internal conversion coefficients, defined as the ratio between electron and γ-emission rates, were determined by simultaneously measuring the γ radiation and the conversion electrons.

γ rays were recorded by a coaxial HPGe detector Compton suppressed and conversion electrons by a miniorange spectrometer (MOS). The coaxial HPGe detector, which had an energy resolution of 2 keV at 1332 keV, was positioned at 90° with respect to the beam direction. The miniorange spectrometer [14] consists of a magnetic lens [made by permanent neodymium iron boron (NdFeB) magnets with an external cladding of nickel copper nickel] and of a Canberra ESLB 500–5000 Si(Li) detector, 5-mm thick and 500 mm^2 in area, cooled to liquid-nitrogen temperature. It was placed at 45° with respect to the beam in the backward direction. Since conversion coefficients are deduced from the ratio of the γ-ray and electron intensities, it is important to calibrate the efficiency of the detectors. The energy and efficiency calibrations of the HPGe detector were measured by using ^{152}Eu and ^{207}Bi sources placed in the target position. A further check was possible by using the known relative γ-ray intensities of the nuclei populated in the experiment.

The energy resolution of the MOS is entirely due to the properties of the silicon detector and was ≈6.5 keV at 900 keV. The magnetic field produced by the permanent magnets has the only purpose of filtering and transporting the electrons to the detector. The efficiency of the MOS is, therefore, strongly energy dependent. The position and the width of the transmission window depend on the type and number of the magnets and on the distance between the magnets and the source and between the magnets and the silicon detector. Since the 0_2^+ state in ^{162}Yb lies at 1006 keV, we choose a transmission window that ranges from ≈500 keV up to ≈1300 keV with a maximum transmission around 1000 keV.

B. The MOS transmission curve

To reduce the uncertainty due to the MOS efficiency as much as possible, the transmission curve has been measured by using different complementary approaches: (i) the spectrum of a ^{90}Sr β^- source was recorded with the same magnetic lens and distances as in the experiment and without the magnetic lens; (ii) the conversion electrons of the decay transitions of a ^{207}Bi source were measured with and without a magnetic lens; (iii) an off-beam measurement was performed by using the ^{11}B + ^{197}Au reaction at $E_{\text{beam}} = 56$ MeV that populates ^{203}Po and ^{204}Po, which decay into ^{203}Bi and ^{204}Bi, respectively, and subsequently into ^{203}Pb and ^{204}Pb; γ rays were also recorded at the same time, and transitions with known conversion coefficients were analyzed and were used as reference points; (iv) known $E2$ transitions or with known conversion coefficients in the nuclei produced in the ^{19}F + ^{147}Sm reaction were used.

The measurements of the ^{90}Sr spectra were performed at the University of Camerino by using a precise reproduction of the experimental setup used at LNS. Since no good energy resolution is required, a Canberra LEC 500–5000 Si detector was used for simplicity. This detector has the same geometry as the one used during the experiment, it works at room temperature and has an energy resolution of ≈25 keV. The use of a continuum β^- source with and without a magnetic lens directly gives the shape of the transmission curve, but it requires a correction due to the backscattering of the electrons in the detector: Since the trajectories of slow electrons have larger angles with the magnets than without and since the percentage of backscattered particles depends upon their incoming angle, a different dependence on energy is expected with and without magnets. This is true whatever source is used, both continuum and discrete, but whereas, in the latter case the background originating from this effect can be easily subtracted, in the case of a continuum source it overlaps with the true events and cannot be distinguished. The correction was made empirically following the procedure suggested by

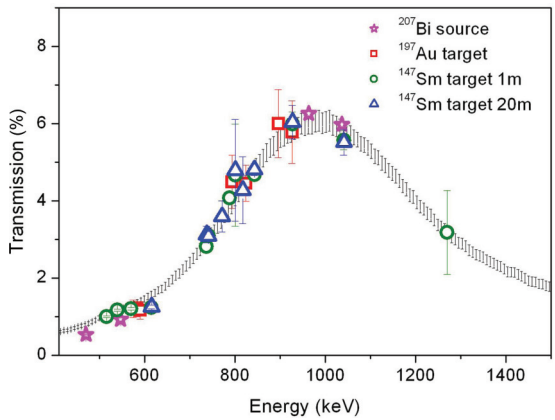

FIG. 2. (Color online) The transmission curve of the MOS obtained by dividing the spectra of a ^{90}Sr source recorded with and without a magnetic lens. Points are obtained from transitions with known conversion coefficients in the 1 min ("1m") and 20 min ("20m") spectra of the experiment and in the calibration run on the Au target (see text).

Farzin *et al.* [15], and we use the same notation for simplicity. The authors assumed the fraction of backscattered electrons, denoted by k, constant with energy in the case of no magnets [$k(E) = k0$], whereas, in the presence of the magnetic field it was assumed to be $k(E) = k0$ for $E > E0$, which corresponds to electron trajectories with an incident angle still close to 90° and a linear dependence on energy from $k(E0) = k0$ to $k(E = 0) = k_m$, which corresponds to trajectories more and more bent by the magnetic field. The values of E_0, k_0, and k_m are then adjusted as explained further in the text. The transmission curve is then given by the expression [15],

$$T(E) = \frac{N_{mw}(E) - N_{scw}(E)}{N_{m0}(E) - N_{sc0}(E)}(1 - k_0),$$

where N_{mw} is the measured spectrum with magnets, N_{scw} is the spectrum due to events in which part of the incident electron energy is lost due to backscattering with magnets and N_{m0} and N_{sc0} are the corresponding spectra with no magnets. At each energy, the measured rate of events is given by the true rate N_{tw}, minus the events scattered into lower channels plus the events scattered from higher channels: $N_{mw}(E) = N_{tw}(E)(1–k) + N_{scw}(E)$ and similarly in the case of no magnets. The rates N_{sc} are determined by starting from the end point of the β source where no N_{sc}'s contribute and by calculating the N_t true rate at lower energies with a recursion procedure. E_0, k_0, and k_m were adjusted to simultaneously reproduce the background due to backscattering in the spectrum of ^{207}Bi recorded with the magnets (N_{scw}) and the ratio of the areas of the peaks of ^{207}Bi observed with and without magnets. The values obtained are as follows: $E_0 = 1200$ keV, $k_0 = 0.30$, and $k_m = 0.45$. The correction mostly affects the low-energy part of $T(E)$.

The resulting empirical transmission curve $T(E)$ is plotted in Fig. 2. The error obtained with this method is about 3% for energies up to about 1 MeV and increases to 5% at around 1.3 MeV due to the lower statistics. In Fig. 2, the experimental points obtained with the approaches (ii)–(iv) described above are plotted. Approaches (iii) and (iv) suffer from larger errors due the experimental error in the known conversion coefficients together with uncertainties due to doublets and the mixture of K and L components in the electron spectrum. We, therefore, used these approaches essentially as a normalization check.

C. The reaction

Levels of ^{162}Yb were populated by EC decay of ^{162}Lu: ^{162}Lu(1.37 min) → ^{162}Yb. ^{162}Lu was produced by the ^{147}Sm (^{19}F,4n) fusion evaporation reaction at $E_{\text{beam}} = 95$ MeV; the ^{19}F beam was provided by the LNS Tandem Accelerator in Catania. The self-supporting target was ∼1.1-mg/cm^2 thick.

A beam-pulsing device, which consisted of a fast switching shutter, was used to irradiate the target at fixed intervals. In our case the on/off period was set to 1 min/1 min, and data were taken only during beam-off intervals. ^{162}Yb decays into ^{162}Tm (lifetime of 18.9 min) and ^{162}Tm into ^{162}Er (lifetime of 21.7 min). Furthermore, in this reaction other unstable nuclei are expected to be populated [16]. They are listed in Table I together with their decaying chains. All these unstable nuclei decay via EC, therefore, only conversion electrons of transitions that depopulate excited states contribute to the electron spectrum. Not all nuclei listed in Table I, however, contribute to the off-line spectra since nuclei that decay only to the ground state of their daughter nucleus will not emit γ rays or conversion electrons. In our case, besides transitions of ^{162}Yb, several intense γ transitions of ^{162}Er are observed up to 1400 keV. Other nuclei involved in the decay processes contribute with only one or two strong transitions: 599.9 and 631.5 keV in ^{161}Tm, 163.3 keV in ^{162}Tm, 860.3 keV in ^{163}Tm, 624.5 and 649.1 keV in ^{159}Ho, and 826.6 keV in ^{161}Ho. The relative intensities of the γ transitions populated

TABLE I. Nuclei expected in the reaction and their decay chains. All data are taken from Ref. [17].

Nuclei produced in the reaction	Relative production	β^+/EC				
^{163}Lu (4 min)	3%	→ ^{163}Yb (11 min)	→ ^{163}Tm (1.8 h)	→ ^{163}Er (75 min)	^{163}Ho	
^{163}Yb (11 min)	1%	→ ^{163}Tm (1.8 h)	→ ^{163}Er (75 min)	→ ^{163}Ho		
^{162}Lu (1.4 min)	50%	→ ^{162}Yb (19 min)	→ ^{162}Tm (22 min)	→ ^{162}Er		
^{162}Yb (19 min)	27%	→ ^{162}Tm (22 min)	→ ^{162}Er			
^{161}Lu (77 s)	4%	→ ^{161}Yb (4 min)	→ ^{161}Tm (30 min)	→ ^{161}Er (3.2 h)	→ ^{161}Ho (2.5 h)	→ ^{161}Dy
^{161}Yb (4 min)	2%	→ ^{161}Tm (30 min)	→ ^{161}Er (3.2 h)	→ ^{161}Ho (2.5 h)	→ ^{161}Dy	
^{159}Tm (9 min)	9%	→ ^{159}Er (36 min)	→ ^{159}Ho (33 min)	→ ^{159}Dy		

in these nuclei via EC decay are all known, therefore, it is possible to monitor possible non-negligible contaminations in transitions of interest. In particular, the 631.8-keV transition of ^{162}Yb overlaps with the 631.5-keV one of ^{161}Tm, the 798.6-keV one corresponds both to a transition in ^{162}Yb and to one in ^{162}Er, and the 825.3-keV transition of ^{162}Yb lies very close to the 826.6-keV one of ^{161}Ho. As can be seen in Table I, ^{162}Lu together with ^{161}Lu have the shortest lifetimes of approximately 1 min. ^{163}Lu and ^{161}Yb have lifetimes of 4 min. All the other nuclei involved in the reaction have longer lifetimes. Therefore, by allowing the shutter to switch over longer times, a different relative population can be obtained in the spectra, and this can be used to disentangle the contribution of ^{162}Yb from the other nuclei. For this purpose, we also measured a γ spectrum and an electron spectrum with an on/off beam time of 20 min/20 min. In this way, long lifetime nuclei will be enhanced in the spectra. In Fig. 3, the two γ spectra obtained with on/off 1 and 20 min are compared. In spectrum (a), recorded with an on/off beam time of 1m, transitions that belong to ^{162}Yb are more intense, whereas, in spectrum (b), recorded with an on/off beam time of 20m, γ rays from longer living nuclei are prominent. We can then subtract from the 1m γ spectrum the 20m one, normalized in such a way that ^{162}Er transitions are canceled and can obtain the spectrum "1m20" shown in the upper part of Fig. 4 where only short lifetime decays are left, and in particular, only γ transitions of ^{162}Yb are present in the energy region of interest from 700 to 1200 keV. Similarly, by subtracting the 1m spectrum from the 20m one, normalized to cancel ^{162}Yb, the spectrum in the bottom part of Fig. 4 is obtained (20m1). In Tables II and III the intensities of the γ transitions of ^{162}Yb and ^{162}Er, respectively, deduced from these γ spectra are compared with the ones known in literature. In Table II, the intensity of the 631.7-keV γ transition has been calculated by subtracting the intensity of the 631.5-keV one of ^{161}Tm taken from literature and normalized to the 599.9-keV transition of ^{161}Tm. In both Tables II and III, the intensity of the γ ray at 798.6 keV has been partitioned to ^{162}Yb and ^{162}Er according to the relative population of the two nuclei in the spectra.

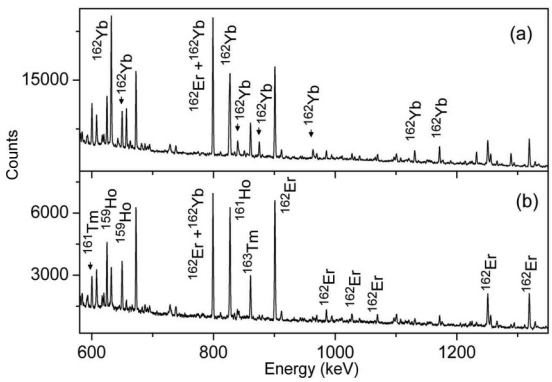

FIG. 3. (a) γ spectrum 1m recorded with the on/off shutter time 1 min/1 min, (b) γ spectrum 20m recorded with the on/off shutter time 20 min/20 min.

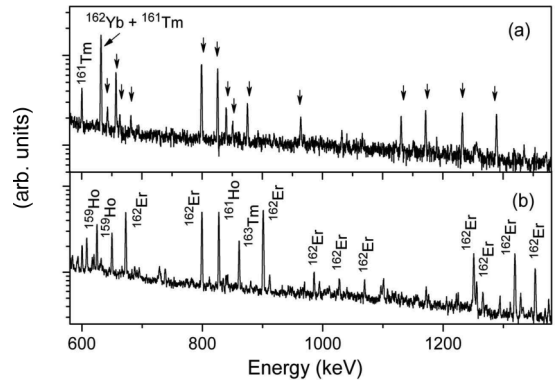

FIG. 4. (a) γ spectrum 1m20 obtained by subtracting the 20m spectrum normalized to the ^{162}Er transitions from the 1m spectrum. Above 650 keV only transitions of ^{162}Yb, indicated by an arrow, are observed. (b) γ spectrum 20m1 obtained by subtracting the 1m spectrum normalized to the ^{162}Yb transitions from the 20m spectrum. Spectra are drawn on a logarithmic scale for a better view.

D. Results and discussion

All γ and electron spectra, 1m, 20m, 1m20, and 20m1, have been analyzed to check consistency in the measured conversion coefficients. The electron spectra are shown in Figs. 5 and 6. A partial level scheme of ^{162}Yb that shows the observed transitions can be seen in Fig. 1. In the 20m spectra [see Figs. 3(b) and 5(b)], the relative population of ^{162}Yb is rather small compared to the population of all other nuclei and, especially, ^{162}Er. Therefore, only intense transitions could be analyzed for ^{162}Yb in these spectra. In general, the number of nuclei populated and the unfortunate overlap of transitions with the same energy makes the analysis rather difficult. In Table IV, the conversion coefficients α_K of transitions in ^{162}Yb deduced from this experiment are listed and are compared with previous data when present. In the same table, the conversion coefficients for transitions in ^{162}Er, ^{161}Ho, and ^{163}Tm are also listed.

TABLE II. γ intensities for some transitions of ^{162}Yb, normalized to the 167-keV transition.

Energy (keV)	Reference [18]	1m	20m	1m20
320.6	16.7 ± 0.2	16.7 ± 0.4	16.9 ± 0.4	15.5 ± 0.4
631.7[a]	22.3 ± 0.3	20.7 ± 1.2[a]	22.2 ± 1.2[a]	22.8 ± 0.4[a]
798.5[b]	14.3 ± 0.2	14.3 ± 1.2[b]	14.2 ± 1.2[b]	14.2 ± 0.3
825.3	11.6 ± 0.3	11.8 ± 0.4	12.7 ± 0.9	11.6 ± 0.3
839.4	3.3 ± 0.2	<3.8 ± 0.4		3.2 ± 0.3
874.8	4.3 ± 0.2	4.4 ± 0.4	5.0 ± 0.8	4.4 ± 0.3
962.9	2.7 ± 0.1	3.2 ± 0.4	4.3 ± 2.1	3.2 ± 0.2
1129.7	3.6 ± 0.2	3.2 ± 0.4		4.3 ± 0.4
1170.6	4.9 ± 0.2	4.9 ± 0.8		5.5 ± 0.4
1231.5	4.6 ± 0.2	5.1 ± 0.6		5.6 ± 0.4
1288.2	5.4 ± 0.2	5.2 ± 0.5		5.9 ± 0.4

[a]The γ line is a doublet; the intensity of the 631.5-keV transition of ^{161}Tm has been estimated as explained in the text.
[b]The γ line is a doublet; the intensity of the 798.7-keV transition of ^{162}Er has been estimated as explained in the text.

TABLE III. γ intensities for some transitions of ^{162}Er, normalized to the 227-keV transition. Errors are statistical in all spectra.

Energy (keV)	Reference [18]	1m	20m	20m1
570.7	27.4 ± 2.2 } 30.1 ± 2.9	30.5 ± 2.5	34.8 ± 3.2	37 ± 3.3
571.2	2.7 ± 1.9 }			
672.3	78 ± 4 } 103.9 ± 4.4	93.0 ± 7.2	94.8 ± 8.2	95.8 ± 8.1
672.4	25.9 ± 1.8 }			
798[a]	10.8 ± 1.5 } 128.8 ± 4.3	119.8 ± 9.7	128 ± 11.0	127.4 ± 10.6
798.7[a]	118 ± 4.0 }			
821.5	4.5 ± 0.4	3.5 ± 1.1	4.5 ± 0.5	4.4 ± 0.5
841.4	9.2 ± 0.5	9.9 ± 0.8	10.9 ± 1.1	12.3 ± 1.2
899.9	79 ± 5.0 } 170 ± 6.4	166.5 ± 12.7	172.3 ± 14.4	171.2 ± 14.1
900.7	91 ± 4.0 }			
985.1	16.2 ± 0.7	17.3 ± 1.4	20.1 ± 1.9	20 ± 1.9
1069.1	15.5 ± 0.8	15.6 ± 1.3	15.4 ± 1.5	14 ± 1.4
1099	19.3 ± 1.0	21.2 ± 1.8	21.3 ± 2.0	22.3 ± 2.1
1250	67.8 ± 2.5	63.5 ± 5.1	70.2 ± 6.0	71.8 ± 6.1
1254.7	20.5 ± 1.5	29.3 ± 8.8	25.2 ± 2.4	24.2 ± 2.2
1318.4	70 ± 3.0	78.3 ± 6.2	77.7 ± 6.6	78.2 ± 6.2
1328	12.3 ± 1.0		12.3 ± 1.4	12.8 ± 1.3

[a]The γ line is a doublet; the intensity of the 798.7-keV transition of ^{162}Er has been estimated as explained in the text.

1. The 631-keV transition

The 631.87-keV $E2$ transition deexcites the 2_2^+ level in ^{162}Yb at 789.4 keV, assigned to the γ band. It overlaps with the 631.45 keV $M1(+E2)$ transition in ^{161}Tm with the known conversion coefficient (0.013). Relative contributions can be separated because of known γ intensities. K electrons differ by 2 keV, not enough to be separated. Furthermore, at the same energy the contribution of the 624-keV transition of ^{159}Ho also has to be taken into account. Therefore, only the 1m spectrum is clean enough to deduce conversion coefficients.

2. The 825-keV transition

This transition deexcites the 3^+ level of ^{162}Yb at 992 keV to the 2_1^+ state. The 827-keV $M1$ transition of ^{161}Ho can easily be separated in the γ spectra. The corresponding K electron energies are 764 and 771 keV, respectively, and these peaks can be fitted separately in the electron spectra.

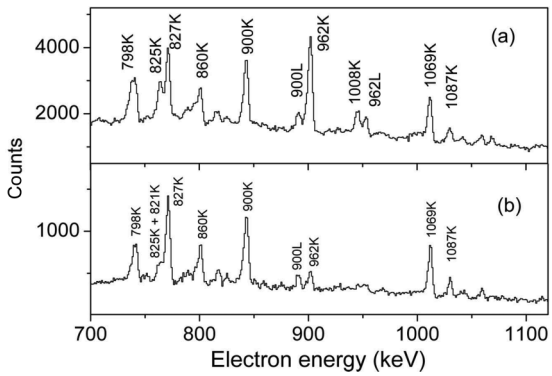

FIG. 5. (a) Electron spectrum 1m recorded with the on/off shutter time 1 min/1 min, (b) electron spectrum 20m recorded with the on/off shutter time 20 min/20 min.

However, we should take the presence of the 821-keV transition in ^{162}Er into account, which is expected to be populated rather weakly, but could be not negligible, especially, in the 20m spectra. The 821-keV transition has unknown multipolarity, and the corresponding K electron energy is 764 keV. This could explain the difference in the conversion coefficient values obtained for the 825-keV transition from the 1m, 20m, and 1m20 spectra. In the last case, where no contribution of ^{162}Er is expected, the value obtained is consistent with an $E2$ transition, but a $M1$ mixing cannot be excluded.

3. The 798-keV transition

At this energy, two strong transitions are present in ^{162}Yb and ^{162}Er, both of multipolarity $E2$. The γ energy is so close

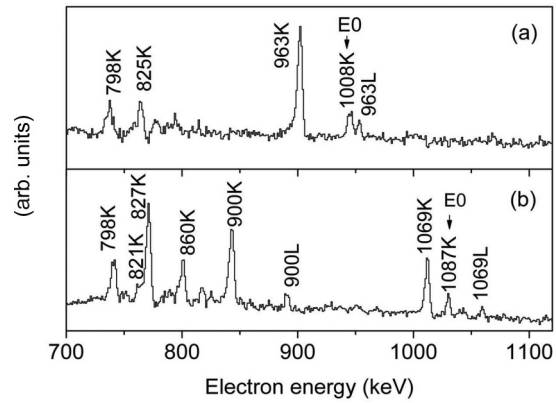

FIG. 6. (a) Electron spectrum 1m20 obtained by subtracting the 20m spectrum from the 1m spectrum. Only transitions of ^{162}Yb are observed. (b) Electron spectrum 20m1 obtained by subtracting the 1m spectrum from the 20m spectrum. No ^{162}Yb transitions are observed.

TABLE IV. Internal conversion coefficients α_K for transitions in ^{162}Yb. For the 962.9-keV transition α_L also is given.

Nucleus	Energy (keV)	Multipolarity	Reference [18]	1m	20m	1m20	20m1
^{162}Yb	631.9	$E2$	0.008 14(12)			0.0104(9)	
^{162}Yb	798.8	$E2$	0.004 89(7)	0.0044(4)	0.0049(6)	0.0052(6)	
^{162}Yb	825.3			0.0065(6)	0.0149(16)[a]	0.0055(6)	
^{162}Yb	963	$(E2)$	0.0033(5)[b]	0.042(6)	0.031(6)[c]	0.040(7)	
^{162}Yb	963	$(E2)$	0.000 530(8)[b,d]	0.008[d] (2)	0.008(2)	0.006[d] (3)	
^{162}Yb	1130			0.0026(5)			
^{162}Er	798.6		0.004 49(7)	} 0.0044(5)	} 0.0044(5)		} 0.0049(7)
^{162}Er	798.7	$E2$	0.004 48(7)				
^{162}Er	899.9	$E2$	0.003 49(5)	} 0.0034(4)	} 0.0035(4)		} 0.0038(6)
^{162}Er	900.7	$E2$	0.003 48(5)				
^{162}Er	985.1	$E2$	0.002 90(5)	0.0029(6)	0.0026(5)		0.0030(6)
^{162}Er	1069	$E0+M1+E2$	0.0290(5)	0.024(5)	0.023(4)		0.027(5)
^{162}Er	1100	$E2$	0.002 32(4)	0.0023(5)	0.0027(6)		0.0024(5)
^{162}Er	1250	$E1$	0.000 78(1)		} 0.0016(3)		} 0.0011(3)
^{162}Er	1254.7	$E1$	0.000 77(1)				
^{162}Er	1318.4				0.0011(2)		0.0012(3)
^{162}Er	1328	$E0+M1+E2$	0.008(5)	0.009(1)	0.008(1)		0.006(2)
^{159}Ho	624.4	$M1$	0.015 49(22)				
^{161}Tm	631.5	$M1(+E2)$	0.013(6)			0.013(5)	
^{161}Ho	826.6	$M1$	0.0083(8)	0.0077(7)	0.0081(7)		0.0079(8)
^{163}Tm	860.3	$M1,E2$	0.006(2)	0.0067(7)	0.0069(7)	0.0067(15)	0.0080(9)

[a]Possibly contaminated with the 821-keV transition of ^{162}Er.
[b]$2^+ \rightarrow 2^+$ transition [7], in principle, $E0+M1+E2$ are allowed. We indicate the conversion coefficients expected for a pure $E2$ transition [19].
[c]Possibly contaminated with the 962-keV transition of ^{162}Er.
[d]Internal conversion coefficients α_L for L electrons.

that the transitions cannot be separated. The γ intensity of the peak has been divided according to the tabulated intensities and the relative population of the two nuclei. The corresponding K electron energies are 737 and 741 keV for ^{162}Yb and ^{162}Er, respectively. In this case the energy difference is such that it is possible to fit the peak as a doublet. The procedure produces large errors, but the results are, however, consistent with the multipolarity assignment $E2$.

4. The 839-keV transition

This transition deexcites the 0_2^+ level to the 2_1^+ level, and it would be important to determine its conversion coefficient to deduce the $X(E0/E2)$ value of the the 0_2^+ state. Unfortunately, the γ intensity is rather small, and at very close energies a number of possible contributing γ transitions from other nuclei cannot be excluded, such as, for example, the 834- and 841-keV transitions of ^{162}Er and the 843-keV one of ^{161}Tm. Furthermore, in the electron spectra the K electron peak at 778 keV is affected by the strong K electron peak at 771 keV, which corresponds to the γ transition at 827 keV of ^{161}Ho. In the 1m20 electron spectrum, this last peak is slightly negative since its area is larger in the 20m spectrum than in the 1m one. As a consequence, it is not possible to obtain a reasonable value for the electron intensity of this transition.

5. The E0 decay at 1006 keV

The level at 1006 keV in ^{162}Yb has been given a 0^+ spin assignment by McCutchan *et al.* [7]. No γ transition to the ground state is observed in the γ spectra. In the electron spectra a peak is observed at 945 keV, which corresponds to the K conversion electron of the $E0$ transition. For an $E0$ transition it is not possible to define an internal conversion coefficient. Usually, one defines [20] the dimensionless ratio of the $E0$ and $E2$ reduced transition probabilities $X(E0/E2) = \rho^2(E0)e^2R^4/B(E2)$ or the equivalent experimental value [10],

$$X\,(E0/E2) = 2.54 \times 10^9 A^{4/3} q_k^2 \left(\frac{E0}{E2}\right) \frac{\alpha_K\,(E2)}{\Omega_k\,(E0)} E_\gamma^5,$$

where $\alpha_K(E2)$ is the internal $E2$ conversion coefficient, $\Omega_k(E0)$ is the electronic factor, and $q_k^2\,(E0/E2)$ is the ratio between the $E0$ and the $E2$ K electron intensities $I_K(E0)$ and $I_K(E2)$. In the case of a $0_2^+ \rightarrow 0_1^+$ transition, the $E2$ refers to the $0_2^+ \rightarrow 2_1^+$ decay. In our case, as already mentioned, no information could be obtained for the $E2$ K electron intensity for the transition that deexcites the 0^+ state to the first excited 2^+ state of 839-keV γ energy. Since we observe the transition in the 1m and 1m20 γ spectra and since we know its multipolarity, we can deduce the $E2$ K electron intensity by multiplying the γ intensity by the expected conversion coefficient 0.0044 [19] (method A). When the $0_2^+ \rightarrow 2_1^+$ decay is not observed, one can still deduce q_k^2 from other observed $E2$ intensities (denoted by $E2'$) by means of the relation [10],

$$I_K(E2) = \frac{\alpha_K(E2)}{\alpha_K(E2')} \frac{I_\gamma\,(E2)}{I_\gamma(E2')'} I_K\left(E2'\right),$$

where I_γ denotes the γ intensities. In the spectra 1m20 where no contributions of ^{162}Er are expected, the 798-keV $E2$ transition can be used (method B). Alternatively, one can also consider the 631-keV $E2$ transition, but in this case, care

TABLE V. $X(E0/E2)$ values obtained for the 0^+ state at 1006 keV in ^{162}Yb. Methods A–C are explained in the text.

	$X(E0/E2)$
Spectra 1m20—method A	0.083(42)
Spectra 1m20—method B	0.075(40)
Spectra 1m20—method C	0.080(42)
Spectra 1m—method A	0.072(71)
Weighted mean	0.078(22)

has to be taken to subtract the contribution of the 631.5-keV transition of ^{161}Tm for which the conversion coefficient is known. Its γ intensity can be evaluated from the intensity of the 599.9-keV line of the same nucleus (method C). In the spectra 1m, although the statistics is higher, for all known $E2$ transitions in ^{162}Yb we cannot exclude the contribution of overlapping transitions from other nuclei. Therefore, it is not possible to deduce $X(E0/E2)$ other than with method A. In Table V, the resulting values are listed together with their weighted mean: $X(E0/E2) = 0.078\ (22)$.

6. The E0 decay at 1087 keV in ^{162}Er

In all electron 1m, 20m, and 20m1 spectra, we observe the transition that corresponds to the $0_2^+ \rightarrow 0_1^+$ decay from the 1087-keV level in ^{162}Er. No γ line is observed in the γ spectra at that energy. The $0_2^+ \rightarrow 2_1^+$ decay at 985 keV is also observed both in the γ and in the electron spectra. An $X(E0/E2)$ value can, thus, be derived in the three cases (see Table VI). The weighted value of $X(E0/E2) = 0.24(6)$ obtained is smaller than the result of the old measurement by de Boer *et al.* [21] of $X(E0/E2) = 0.31(11)$, although the two values lie within the error bars.

III. IBA-1 CALCULATIONS

Nuclear properties, such as strong $E0$ transitions, changes in isotope and isomer shifts, related to mean-square radii, or changes in two-nucleon separation energies, related to masses, can be regarded as fingerprints for shape coexistence [9]. Unfortunately, the measure of $\rho^2(E0)$ requires the lifetime measurement of the 0_2^+ state, which is often very hard to populate with sufficient intensity, as in the case of ^{162}Yb. The commonly used quantity $X(E0/E2)$ is a ratio between two quantities usually rather small: One is the pure $E0$ transition, and the other is the $E2$ transition from the β to the ground-state

TABLE VI. $X(E0/E2)$ values obtained for the 0^+ state at 1087 keV in ^{162}Er.

	$X(E0/E2)$
Spectra 1m	0.23(9)
Spectra 20m	0.25(10)
Spectra 20m1	0.24(9)
Weighted mean	0.24(6)
de Boer *et al.* [21]	0.31(11)

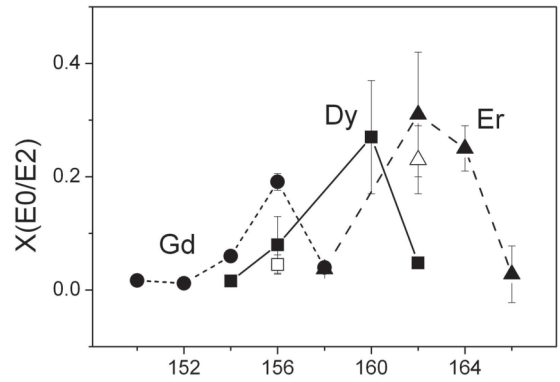

FIG. 7. Known $X(E0/E2)$ values for the Gd (circles), Dy (squares), and Er (diamonds) isotopes. Data are from Ref. [10]; the open square of ^{156}Dy is from Ref. [22]. For ^{162}Er the value found in this paper is also included, indicated by an open diamond. $X(E0/E2)$ is close to zero in spherical nuclei; it increases with deformation by reaching a maximum in deformed nuclei and then decreases again.

band. From a theoretical point of view, it has the disadvantage of implying two parameters related to the $E0$ and the $E2$ operators, respectively. The $E2$ effective charge e_2 can be fixed by fitting the ground-state band $B(E2)$ values, but there are only very few known $E0$ transitions [10], if not only one, such as in ^{162}Yb, or none. In this mass region, $\rho^2(E0)$'s are known only for the Gd isotopes: The value is very small for the spherical ^{146}Gd; it raises up to a maximum for ^{154}Gd, which well approximates X(5), and decreases for heavier isotopes. On the other hand, the $B(E2; 0_2^+ \rightarrow 2_1^+)$ value is large for spherical Gd nuclei and decreases with increasing deformation in such a way that the ratio $X(E0/E2)$ is close to zero for spherical nuclei, it increases with increasing deformation until a maximum when deformation is well settled, and then decreases again as can be seen in Fig. 7. There is, therefore, an indication that the critical point lies in the intermediate region between the minimum $X(E0/E2)$ value on the spherical side and the maximum on the deformed side of the isotope chain. The trend in the $X(E0/E2)$ values is similar for the other isotope chains in the region as shown in Fig. 7. For the Dy isotopes, the X(5) candidate is ^{156}Dy, whereas, in the case of Er, the critical point seems to lie between ^{160}Er and ^{162}Er: ^{160}Er is, in fact, closer to the spherical limit, and ^{162}Er is closer to the rotational one.

Recently, Zerguine *et al.* [11] suggested a relation between the mean-square charge radius and the monopole operators. More precisely, they derived the following expressions:

$$\hat{T}(r^2) = \langle r^2 \rangle_c + \alpha N_b + \eta \hat{n}_d,$$
$$\hat{T}(E0) = (e_n N + e_p Z)\eta \hat{n}_d,$$

where $\langle r^2 \rangle_c$ is the charge radius of the core nucleus. Its contribution disappears when calculating isotope shifts. In fact, isotope shifts are given by the expression,

$$\Delta\langle r^2 \rangle^A = \langle r^2 \rangle^{A+2}_{\text{g.s.}} - \langle r^2 \rangle^A_{\text{g.s.}}$$
$$= \alpha + \eta\left(\langle \hat{n}_d \rangle^{A+2}_{\text{g.s.}} - \langle \hat{n}_d \rangle^A_{\text{g.s.}}\right).$$

The authors also estimated that the parameter α, related to the dimension of the nucleus, should have a value on the

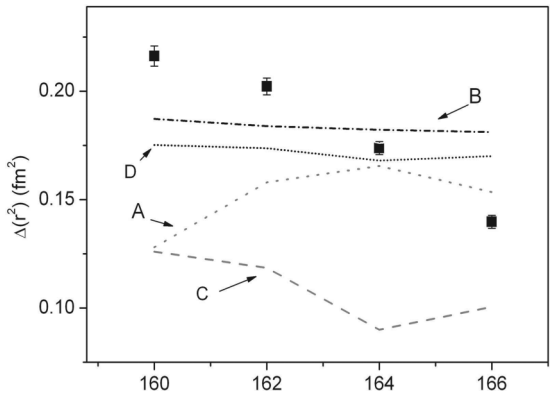

FIG. 8. Calculated Yb isotope shifts are compared with the experimental ones (full circles): A: calculations from Zerguine *et al.* [11]; B: calculations from Chou *et al.* [12]; C: calculations from McCutchan *et al.* [13] use the parameters $\eta = 0.15$ fm^2 and $\alpha = 0$ fm^2; and D: the same as C but with parameters $\eta = 0.03$ fm^2 and $\alpha = 0.15$ fm^2. Data are from Ref. [24].

order of ≈0.2 fm^2 in this mass region, whereas, η, associated with the deformation contribution, should vary from ≈0.02 to ≈0.07 fm^2, from weakly deformed to strongly deformed nuclei.

In the same paper, the authors performed extensive calculations over all isotopes in the $A \approx 150$–170 region from samarium to tungsten by using a multipole expansion of the IBA-1 Hamiltonian and by allowing only the quadrupole parameter to vary along each isotope chain to fit energy spectra. They then applied the calculations to describe isotope shifts and $\rho^2(E0)$ where known. For the effective charges in the monopole operator, the authors found from a fit on charge radii that a reasonable choice was $e_p = e$ and $e_n = 0.5e$. The strict requirement on the parameters went to the detriment of the quality of the fit for the single nuclei, and in particular, for the lighter Yb isotopes the agreement between calculated and experimental energy levels and isotope shifts is not satisfactory: The trend of the isotope shifts is even opposite to the experimental one as can be seen in Fig. 8, curve A. Nevertheless, we extended the same calculations to $X(E0/E2)$ values, which were not considered in that paper by obtaining as a result a far too small value for ^{162}Yb, although the trend follows the expectations as shown in Fig. 9, curve A.

Other extensive calculations were performed in the past in this mass region with the aim of describing the whole region with a small number of smoothly varying parameters. In this way, a predictive power for poorly known nuclei can be tested. Chou *et al.* [12] used the extended consistent Q formalism to describe all collective nuclei that span the $Z = 50$–82 shell. Within this formalism the Hamiltonian has the simple form

$$H = \varepsilon n_d - \kappa Q Q, \tag{1}$$

where

$$Q = (s^+\tilde{d} + d^+ s) + \chi(d^+\tilde{d})^{(2)}. \tag{2}$$

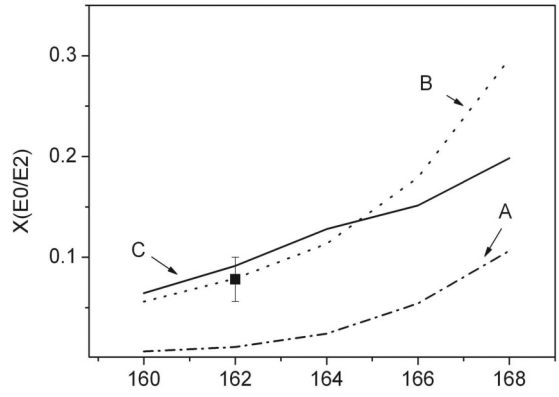

FIG. 9. Calculated $X(E0/E2)$ values are compared with the experimental value of ^{162}Yb measured in this paper: A: calculations from Zerguine *et al.* [11]; B: calculations from Chou *et al.* [12]; and C: calculations from McCutchan *et al.* [13] use the parameter $\eta = 0.03$ fm^2.

The value of κ was kept constant ($\kappa = 0.03$ MeV) for all nuclei by following the suggestion of Ref. [23], and the variation in the two parameters ε and χ to describe energy levels and $B(E2)$ transitions has been analyzed as a function of the nuclear deformation. Overall good results were obtained for the yrast and γ band, but the agreement was only fair for the excited 0^+ states. When applied to describe isomer shifts in the Yb isotopes, the calculations fail to reproduce the experimental trend since the predicted trend is rather flat as can be seen in Fig. 8, curve B. $X(E0/E2)$ values, however, seem to follow the expected trend and agree well with the experimental point in ^{162}Yb (see Fig. 9, curve B).

A slightly different approach was followed by McCutchan *et al.* [13], who used the same Hamiltonian but related the two parameters ε and κ to a new parameter ζ in the following way:

$$H = c\left[(1-\zeta)n_d - \frac{\zeta}{4N_B}QQ\right], \tag{3}$$

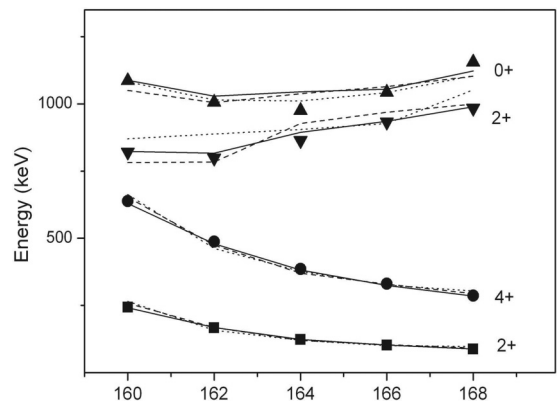

FIG. 10. Comparison between experimental (symbols) and calculated (lines) yrast 2^+ and 4^+ states and 0^+ and 2^+ β band energies of the Yb isotopes. Solid lines refer to the calculations of McCutchan *et al.* [13], dashed lines refer to calculations of Ref. [13] with adjusted parameters to also fit isotope shifts, and dotted lines refer to calculations performed with a general IBA-1 Hamiltonian.

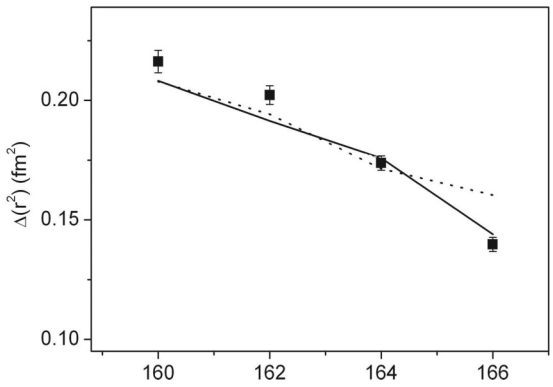

FIG. 11. Calculated isotope shifts are compared with the experimental ones (full circles). The dashed line refers to calculations from McCutchan *et al*. adjusted to reproduce energies and isotope shifts in the Yb isotopes as explained in the text. The solid line refers to calculations performed by using a general IBA-1 Hamiltonian. Data are from Ref. [24].

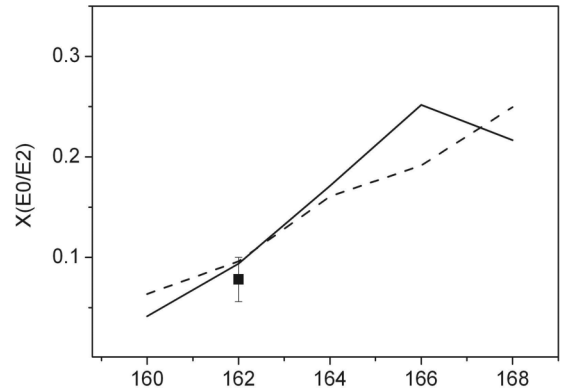

FIG. 12. Calculated $X(E0/E2)$ values are compared with the experimental value of ^{162}Yb measured in this paper: The dashed line refers to calculations from McCutchan *et al*. adjusted to reproduce energies and isotope shifts in the Yb isotopes as explained in the text. The solid line refers to calculations performed by using a general IBA-1 Hamiltonian.

where c is just a scaling factor and Q has the form of Eq. (2). In this way, only two parameters are retained, but all terms in the Hamiltonian are actually varied. Energy levels, transition strengths, two neutron separation energies, isomer and isotope shifts were considered in the fit in the regions of $Z = 64$–72 and $N = 86$–104, also well reproducing the energy of the 0_2^+ states. A mapping of all these nuclei in the symmetry triangle was obtained from which ^{162}Yb results rather away from the critical point by already having a large deformation. Also in this case, however, the isotope shifts are, in general, not well reproduced: The parameters α and η, which best reproduce the Gd data ($\alpha = 0$ fm^2, $\eta = 0.15$ fm^2), fail to fit isomer shifts, and on the other hand, the set of parameters $\alpha = 0.15$ fm^2, $\eta = 0.03$ fm^2, which reproduce the Gd isomer shifts, do not reproduce the large change in the isotope shift in the lighter Gd isotopes. None of the two sets reasonably reproduces the Yb isotope shifts data as can be seen in Fig. 8, curves C and D. For the $X(E0/E2)$ values the first set gives values one order of magnitude too large, whereas, the second set reproduces the ^{162}Yb value (see Fig. 9, curve C).

By using the calculations of McCutchan *et al*. [13] as a starting point, we performed a new calculation for the $^{160-168}$Yb isotopes by adjusting the parameters to improve the fit to the isotope shifts. Energy levels were still reproduced reasonably well as can be seen in Fig. 10 where the experimental energies of the 2_1^+, 4_1^+, 2_γ^+, and 0_β^+ are compared to the calculated ones. Isotope shifts and $X(E0/E2)$ values, fitted by using the parameters $\alpha = 0.137$ and $\eta = 0.065$ fm^2, are shown in Figs. 11 and 12, respectively.

The overall agreement is rather good, and the resulting parameters, listed in Table VII, place the Yb nuclei in the symmetry triangle in positions very close to the ones found by McCutchan *et al*. It is evident that both isotope shifts and $X(E0/E2)$ values are quantities quite sensitive to a fine-tuning of the parameters. Such sensitivity leads to the question of how important could be terms in the Hamiltonian that are usually neglected, i.e., the (LL) term, the octupole term $(d^+\tilde{d})^{(3)}$, or the hexadecapole term $(d^+\tilde{d})^{(4)}$. For this reason, we performed calculations on the $^{160-168}$Yb isotopes by using the most general Hamiltonian as was used by Zerguine *et al*. [11] but by varying all the parameters (see Fig. 13) with the only requirement of a smooth variation to simultaneously reproduce the yrast state energies and $B(E2)$'s, the β and γ band-head energies, and the isotope shifts. The resulting level energies are shown in Fig. 10. In Fig. 11, the calculated isotope shifts are compared to the experimental ones. They are obtained with the parameters $\alpha = 0.135$ and $\eta = 0.06$ fm^2. These values are in good agreement with the values estimated in Ref. [11]. Ground state $B(E2)$ values (not shown) were reproduced by using a quadrupole strength parameter $e^2 = 0.16$ eb, kept constant for all isotopes. The effective charges in the expression of the $E0$ operator were $e_n = 0.5$ and $e_p = 1$ as suggested in Ref. [11]. $X(E0/E2)$ values were then calculated with no further free parameter, and the results are shown in Fig. 12. It can be seen that the calculations reproduce the experimental $X(E0/E2)$ value for ^{162}Yb like the previously discussed calculations but show, however, a different trend that goes to ^{166}Yb where the value is maximum and ^{168}Yb where the value decreases. This behavior reproduces a trend common to Gd, Dy, and Er isotopes (see Fig. 7). This might indicate that terms in the IBM-1 Hamiltonian that are negligible when comparing energies or large $B(E2)$ values play a role when describing quantities related to nuclear shape. Extensive calculations on all isotope chains in this region are needed to enquire into this point.

TABLE VII. Parameters of the Hamiltonian of Eq. (3) used in Ref. [13] to describe the Yb isotopes and adjusted in this paper to reproduce isotope shifts.

A	160	162	164	166	168
N_B	10	11	12	13	14
ζ [13]	0.69	0.72	0.73	0.73	0.74
χ [13]	−0.35	−0.42	−0.52	−0.58	−0.61
ζ (this paper)	0.67	0.73	0.72	0.72	0.73
χ (this paper)	−0.31	−0.40	−0.57	−0.61	−0.63

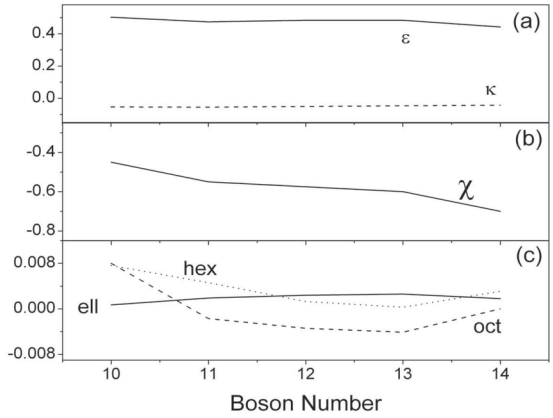

FIG. 13. Variation in the parameters of the general IBA-1 Hamiltonian as a function of boson number N_b. N_b varies from 10 for ^{160}Yb to 14 for ^{168}Yb. (a) Parameters ε and κ [see Eq. (1)], (b) parameter χ [see Eq. (2)], (c) Ell, oct, and hex are the parameters of the (LL), octopole, and hexadecapole operators, respectively. All parameters are in MeV, except for χ, which is dimensionless.

IV. CONCLUSIONS

We measured the conversion electrons for the $E0$ transition $0_2^+ \rightarrow 0_1^+$ in ^{162}Yb by using a MOS. γ rays were measured simultaneously with a high-resolution HPGe detector. To reduce the experimental uncertainty, special care was taken in determining the transmission curve of the MOS using both transitions with known conversion coefficients and a ^{90}Sr β^- source. The $X(E0/E2)$ value of 0.078 ± 0.022 was obtained. Also, in the same experiment, the $0_2^+ \rightarrow 0_1^+$ transition of ^{162}Er was observed, and a new $X(E0/E2)$ value of 0.24 ± 0.06 was obtained to be compared with the previously reported value of 0.31 ± 0.11 [16]. The two values are not in contradiction within the error bars.

We investigated the ability of the IBA-1 model to reproduce $X(E0/E2)$ values by starting from the suggestion of Zerguine *et al.* [11] of relating the mean-square charge radius and the monopole operators. We applied it to few IBA-1 calculations available [11–13] in this mass region to calculate $X(E0/E2)$ values for the $^{160-168}$Yb isotopes. From the results one can conclude that, although gross nuclear features, such as energies and large $B(E2)$ values can be easily reproduced by calculations that use several different simplified approaches within the IBA-1 formalism, properties related to the nuclear shape, such as $E0$ transitions or isotope shifts, are much more sensitive and discriminating since a small variation in the parameters in the Hamiltonian, which do not affect the quality of the fit on energy levels, produce large changes in features related to nuclear shape. In particular, the calculations in Refs. [12,13] reproduce the $X(E0/E2)$ value in ^{162}Yb but predict different values for heavier isotopes. We also performed a new calculation by using the full IBA-1 Hamiltonian and again found good agreement for ^{162}Yb. Furthermore, different from all previous calculations, the $X(E0/E2)$ values reach a maximum value for ^{166}Yb and decrease for ^{168}Yb by following a trend which is observed experimentally in the Gd, Dy, and Er isotope chains. We plan to perform further $E0$ measurements in the neighbor Yb isotopes to investigate the $X(E0/E2)$ trend.

[1] F. Iachello, Phys. Rev. Lett. **85**, 3580 (2000).
[2] F. Iachello, Phys. Rev. Lett. **87**, 052502 (2001).
[3] R. F. Casten and N. V. Zamfir, Phys. Rev. Lett. **87**, 052503 (2001).
[4] D. Tonev, A. Dewald, T. Klug, P. Petkov, J. Jolie, A. Fitzler, O. Moller, S. Heinze, P. von Brentano, and R. F. Casten, Phys. Rev. C **69**, 034334 (2004).
[5] M. A. Caprio, N. V. Zamfir, R. F. Casten, C. J. Barton, C. W. Beausang, J. R. Cooper, A. A. Hecht, R. Krucken, H. Newman, J. R. Novak, N. Pietralla, A. Wolf, and K. E. Zyromski, Phys. Rev. C **66**, 054310 (2002).
[6] E. A. McCutchan, N. V. Zamfir, and R. F. Casten, Phys. Rev. C **71**, 034309 (2005).
[7] E. A. McCutchan, N. V. Zamfir, M. A. Caprio, R. F. Casten, H. Amro, C. W. Beausang, D. S. Brenner, A. A. Hecht, C. Hutter, S. D. Langdown, D. A. Meyer, P. H. Regan, J. J. Ressler, and A. D. Yamamoto, Phys. Rev. C **69**, 024308 (2004).
[8] J. Bonnet, A. Krugmann, J. Beller, N. Pietralla, and R. V. Jolos, Phys. Rev. C **79**, 034307 (2009).
[9] K. Heyde and J. L. Wood, Rev. Mod. Phys. **83**, 1467 (2011).
[10] T. Kibedy and R. H. Spear, At. Data Nucl. Data Tables **89**, 77 (2005).
[11] S. Zerguine, P. Van Isacker, and A. Bouldjedri, Phys. Rev. C **85**, 034331 (2012).
[12] W. T. Chou, N. V. Zamfir, and R. F. Casten, Phys. Rev. C **56**, 829 (1997).
[13] E. A. McCutchan, N. V. Zamfir, and R. F. Casten, Phys. Rev. C **69**, 064306 (2004).
[14] J. van Klinken, S. J. Feenstra, and G. Dumont, Nucl. Instrum. Methods **151**, 433 (1978).
[15] K. Farzin, K. Uebelgunn, and H. von Buttlar, Nucl. Instrum. Methods Phys. Res. A **240**, 329 (1985).
[16] Code PACE4, http://lise.nscl.msu.edu/pace4.html.
[17] Table of radioactive isotopes, http://ie.lbl.gov/toi/.
[18] ENSDF, http://www.nndc.bnl.gov/ensdf/.
[19] http://bricc.anu.edu.au/.
[20] J. O. Rasmussen, Nucl. Phys. **19**, 85 (1960).
[21] F. W. N. de Boer, P. F. A. Goudsmit, B. J. Meijer, P. Koldewijn, J. Konijn, and R. Beetz, Nucl. Phys. A **236**, 349 (1974).
[22] G. Lo Bianco, D. L. Balabanski, S. Nardelli, S. Das Gupta, N. Blasi, K. Gladnishki, A. Saltarelli, and L. Fortunato, J. Phys.: Conf. Ser. **267**, 012054 (2011).
[23] N. V. Zamfir and R. F. Casten, Phys. Lett. B **341**, 1 (1994).
[24] E. Otten, in *Treatise on Heavy-Ion Science, Vol. 8: Nuclei Far From Stability*, edited by D. A. Bromley (Plenum, New York, 1989), p. 517.